

# We are IntechOpen, the world's leading publisher of Open Access books Built by scientists, for scientists

6,900

Open access books available

186,000

International authors and editors

200M

Downloads

Our authors are among the

154

Countries delivered to

TOP 1%

most cited scientists

12.2%

Contributors from top 500 universities



WEB OF SCIENCE™

Selection of our books indexed in the Book Citation Index  
in Web of Science™ Core Collection (BKCI)

Interested in publishing with us?  
Contact [book.department@intechopen.com](mailto:book.department@intechopen.com)

Numbers displayed above are based on latest data collected.  
For more information visit [www.intechopen.com](http://www.intechopen.com)



# Biomimetic Hydroxyapatite Deposition on Titanium Oxide Surfaces for Biomedical Application

Wei Xia<sup>1,2</sup>, Carl Lindahl<sup>1,2</sup>, Jukka Lausmaa<sup>2,3</sup> and Håkan Engqvist<sup>1,2</sup>

<sup>1</sup>*Ångström Laboratory, Department of Engineering Sciences, Uppsala University, Uppsala*

<sup>2</sup>*BIOMATCELL, VINN Excellence Center of Biomaterials and Cell Therapy, Gothenburg*

<sup>3</sup>*Department of Chemistry and Materials Technology, SP Technical Research Institute of Sweden Sweden*

## 1. Introduction

Titanium is widely used as material for permanent implants in orthopedic and dental applications. It is well known that Ti shows a mechanically stable interface towards bone (osseointegration). The good biological properties are due to the beneficial properties of the native oxide (TiO<sub>2</sub>) that forms on Ti when exposed to oxygen. The native titanium oxide on Ti is usually amorphous and very thin, 2-7 nm [1-3]. In addition to being stable in the physiological environment, titanium oxides increase calcium ion interactions, which are important for protein and subsequent osteoblast adhesion [4].

Enhanced bone bonding can be achieved with bioactive materials that form a stable unit with bone through a spontaneous formation of hydroxyapatite (HA) on their surface. The biomineralized HA layer acts as a bonding layer to the bone and integration at the atomic/molecular scale can develop. For this reason HA is proposed as a suitable coating material to provide stronger early fixation of uncemented prostheses. Although hydroxyapatite coatings on implants showed long-term survival [5], there are concerns about their reliability under loads. Possible ways to overcome this lack of mechanical stability could be by reinforcing the HA with metal oxides such as zirconia and alumina [6].

Apatites, as well as other calcium phosphates (CaPs), can occur in different phases, summarized in **Table 1** [7]. Most of them have been studied as biomaterials. The HA naturally occurring in bone is a multi-substituted calcium phosphate, including traces of CO<sub>3</sub><sup>2-</sup>, F<sup>-</sup>, Mg<sup>2+</sup>, Sr<sup>2+</sup>, Si<sup>4+</sup>, Zn<sup>2+</sup>, Li<sup>+</sup> etc [8, 9]. These ionic substitutions are considered to play an important role for the formation and properties of bone.

Hydroxyapatite coatings can be produced by different methods [10-19]. Early attempts used plasma spraying, which however resulted in coatings with adhesion problems. Attempts have also been made with physical vapour deposition (PVD) techniques. Both of these methods suffer from the drawback that they are line-of-sight methods, which means that coating of complex implant geometries is technically difficult. The biomimetic way to

fabricate apatite coatings on implants overcomes these drawbacks. Biomimetic HA coating is, basically, a solution-based method carried out at ambient temperature mimicking body surroundings. The method allows deposition of CaP coatings on many different objects, such as sponges, cements, metal surfaces or fixation rods [20]. Biomimetic deposition of coatings also gives a possibility of co-precipitating ions, drugs, macromolecules and biological molecules together with the inorganic layer. Typically, the substrates with active surfaces are immersed in a simulated body fluid at physiological pH and temperature (approximately 37°C), and an apatite layer will automatically form, crystallize and grow on the surfaces. By varying the immersion conditions, coatings with a wide range of morphologies, thicknesses and composition can be prepared.

In this chapter, some recent developments in biomimetic HA coatings will be reviewed. In section 2 we provide an overview of different types of HA produced by biometric methods. Since biomimetic coating properties are dependent on the substrate properties, some basic properties of titanium (oxide) surfaces are described in section 3. In section 4 we briefly describe some new techniques for studying the formation and properties of biomimetic HA coatings. Sections 5 and 6 provide an overview of recent studies of HA formation on different titanium oxide surfaces, and of ion substituted biomimetic HA coatings, respectively. Finally, section 7 discusses some biological properties of biomimetic HA coatings, and in section 8 we summarize and discuss some directions for the future.

## 2. Selected properties of HA coatings

The standard way of producing biomimetic coatings has for a long time been based on the simulated body fluid (SBF) solutions described by Kokubo [21]. Recently, in order to improve the coating process, the composition of the solutions used for biomimetic HA coatings has been modified (**Table 2**). Except for the inorganic components, some other organic components, such as protein and lactic acid, have been added into SBF [22, 23]. The immersion temperature has also been expanded to temperatures from 4 to 65 °C [23-25]. Based on these biomimetic methods, the resulting apatite coatings will be either amorphous calcium phosphate (ACP), octacalcium phosphate (OCP) or hydroxyapatite (HA). The crystal structures of OCP and HA are shown in **Fig. 1 and 2** [26, 27]. Typical HA is a hexagonal phase, which contains two different cation sites, Ca(I) and Ca(II). A unit cell accommodates a formula unit  $\text{Ca}_{10}(\text{PO}_4)_6(\text{OH})_2$ . Among the 10 cations, the 4 Ca(I)s are tightly bonded to 6 oxygens and less strongly to the other 3 oxygens, whereas the 6 Ca(II) atoms are surrounded by 7 oxygens. OCP ( $\text{Ca}_8(\text{HPO}_4)_2(\text{PO}_4)_4 \cdot 5\text{H}_2\text{O}$ ) has a triclinic structure. Six of the  $\text{Ca}^{2+}$  ions and two of the phosphate groups are hosted in a layer (apatite layer) where they occupy almost the same positions as in HA structure, as shown in **Fig. 2**. Due to its structural features, OCP is often found as an intermediate phase during the precipitation of the thermodynamically more stable HA [26].

Bigi and his co-workers recently summarized ionic substitutions as a tool to improve the biological performance of calcium phosphate based materials [27]. Biomimetic ion substituted hydroxyapatite could therefore not only act as a bonding layer but also further strengthen the bonding and stimulate bone formation.

Investigations of the growth, boundary conditions and surface chemistry of biomimetic hydroxyapatite deposition on titanium oxide surfaces (amorphous and crystalline) can contribute to the understanding of the mechanism of the hydroxyapatite formation *in vivo*. Furthermore, such studies provide a means to grow different HA coatings under controlled biomimetic conditions [24].

Abbreviation	Formula	Name (mineral)	Ca/P ratio	pK <sub>sp</sub> (25 °C) <sup>a</sup>	pH stability <sup>a</sup>	Occurrence in biological tissues
HA	Ca <sub>10</sub> (PO <sub>4</sub> ) <sub>6</sub> (OH) <sub>2</sub>	Hydroxyapatite	1.67	116.8	9.5–12	Bone, dentin, enamel, dental calcifications, urinary stones, atherosclerotic plaques
OCP	Ca <sub>8</sub> H <sub>2</sub> (PO <sub>4</sub> ) <sub>6</sub> ·5H <sub>2</sub> O	Octacalcium phosphate	1.33	96.6	5.5–7.0	Dental and urinary calculi
β-TCP	Ca <sub>3</sub> (PO <sub>4</sub> ) <sub>2</sub>	β-Tricalcium phosphate (whitlockite)	1.5	28.9	<sup>b</sup>	Dental and urinary calculi, soft-tissue deposits, arthritic cartilage, usually present as β-TCP
α-TCP	Ca <sub>3</sub> (PO <sub>4</sub> ) <sub>2</sub>	α-Tricalcium phosphate	1.5	25.5	<sup>b</sup>	Not found
ACP	Ca <sub>x</sub> (PO <sub>4</sub> ) <sub>y</sub> ·nH <sub>2</sub> O	Amorphous calcium phosphate	1.2–2.2	<sup>c</sup>	<sup>b</sup>	Soft-tissue calcifications
MCPM	Ca(H <sub>2</sub> PO <sub>4</sub> ) <sub>2</sub> ·H <sub>2</sub> O	Monocalcium phosphate monohydrate	0.5	1.14	0–2	Not found
MCPA	Ca(H <sub>2</sub> PO <sub>4</sub> ) <sub>2</sub>	Anhydrous monocalcium phosphate	0.5	1.14	<sup>b</sup>	Not found
DCPD	CaHPO <sub>4</sub> ·2H <sub>2</sub> O	Dicalcium phosphate dihydrate (brushite)	1.0	6.59	2–6	Dental calculi, urinary stones, chondrocalcinosis
DCPA	CaHPO <sub>4</sub>	Anhydrous dicalcium phosphate (monetite)	1.0	6.90	<sup>b</sup>	Not found
TTCP	Ca <sub>4</sub> (PO <sub>4</sub> ) <sub>2</sub>	Tetracalcium phosphate	2.0	38–44	<sup>b</sup>	Not found
CDHA	Ca <sub>10-x</sub> (HPO <sub>4</sub> ) <sub>x</sub> (PO <sub>4</sub> ) <sub>6-x</sub> (OH) <sub>2-x</sub>	Calcium-deficient hydroxyapatite	1.5	85.1	6.5–9.5	Not found

<sup>a</sup> Data from ref. [8]

<sup>b</sup> Phase obtained by solid-state reaction or heat treatment of other phases [7]

<sup>c</sup> Cannot be measured precisely, however the following values were reported: 25.7 (pH 7.40), 29.9 (pH 6.00), 32.7 (pH 5.28) [28].

Table 1. Properties and occurrence of the biologically relevant phosphates. [7]

Ion	Na <sup>+</sup>	K <sup>+</sup>	Mg <sup>2+</sup>	Ca <sup>2+</sup>	Cl <sup>-</sup>	HPO <sub>4</sub> <sup>2-</sup> / H <sub>2</sub> PO <sub>4</sub> <sup>-</sup>	SO <sub>4</sub> <sup>2-</sup>	HCO <sub>3</sub> <sup>-</sup>
Blood plasma[29]	142.0	5.0	1.5	2.5	103.0	1.0	0.5	27
SBF[21, 23]	142.0	5.0	1.5	2.5	148.5	1.0	0.5	4.2
PBS[24, 25, 30, 31]	145.0	4.2	0.49	0.91	143	9.6	-	-
5×SBF[32]	710	25	7.5	12.5	741	5	2.5	21
10×SBF[33]	1000	5	5	25	1065	10	-	-
HBSS[34]	141.7	5.7	0.8	1.7	145.6	0.7	0.8	4.2

HBSS: Hanks balanced salt solution

Table 2. Inorganic composition of blood plasma and different simulated body fluids (mM)

### 3. Surface chemistry of titanium oxide

The native titanium oxide formed during normal ambient conditions on Ti is amorphous if there is no additional treatment. In addition to the amorphous phase, three different crystalline phases of titanium dioxide exist naturally, namely rutile, anatase and brookite. **Table 3** summarizes the reported values of isoelectric point (IEP) and point-of-zero charge (PZC) for some titanium dioxides. As can be seen, for both amorphous and crystalline titanium dioxide both the IEP and PZC are in all cases lower than 7. This is very important for hydroxyapatite formation on titanium dioxide in the body simulated fluid (SBF). Because the pH of SBF is  $\sim 7.4$ , the lower IEP could lead to a deprotonation of the titanium oxide surface and the formation of negative Ti-O<sup>-</sup> groups in SBF. The adsorption and dissociation of water can also produce Ti-OH groups and a negative surface charge.

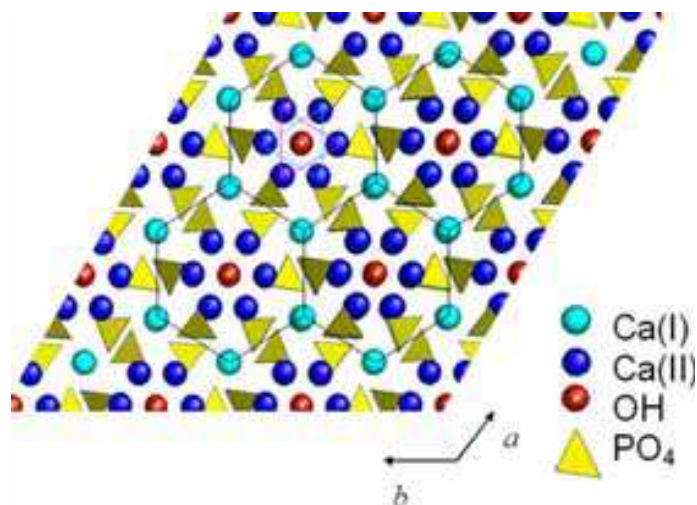


Fig. 1. HA structure along the c-axis. Black lines connect Ca(I) columns in hexagonal networks. Cyan and magenta triangles connect staggered Ca(II) atoms lying in the same plane, but at different height with respect to the c-axis.[27]

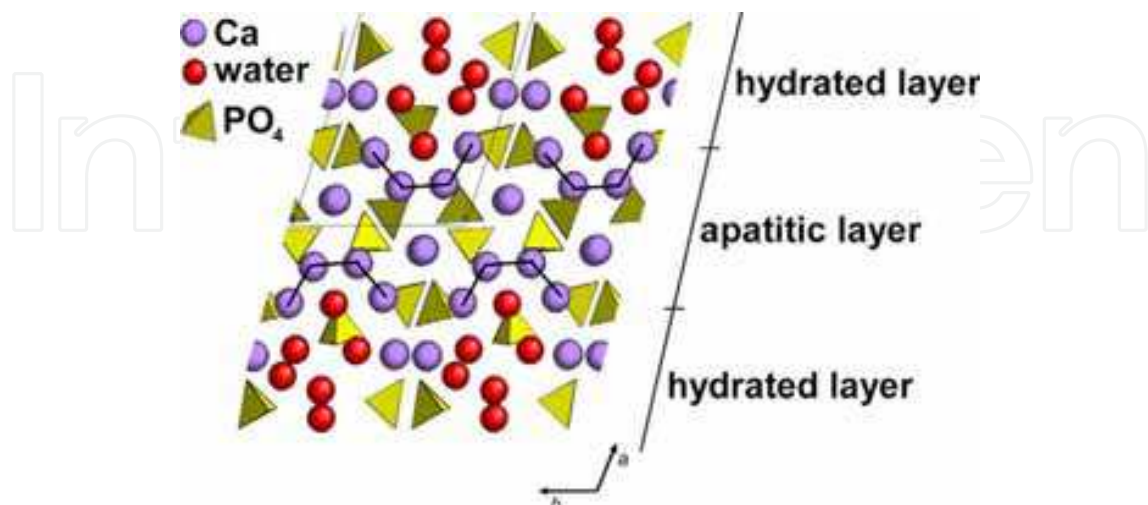


Fig. 2. OCP structure down the c-axis. The hydrated and apatitic layers are highlighted. The positions of Ca atoms connected by black lines and of the phosphate groups of the apatitic layer are very close to those found in the HA structure.[27]

Type of TiO <sub>2</sub>	PZC	IEP
Hydrous TiO <sub>2</sub>	5.0 [35]	5.0 [35]
Nanocrystalline	5.7 [36]	-
Anatase	6.2 [37], 6 [38]	6.2 [39], 5.6 [40]
Rutile	5.5 [38], 5.3 [37]	-

Table 3. Literature values for the point of zero charge (PZC) and iso-electric points (IEP) of TiO<sub>2</sub>

Sol-gel derived amorphous titanium oxide [41] is not considered to be bioactive in the sense that it forms HA on its surface, despite the fact that the IEP is much lower than that of SBF. The crystalline phases of titanium dioxide, anatase and rutile, have good ability to induce hydroxyapatite formation on the surface. However, titanium dental implants with native amorphous surface oxide have shown good osseointegration and been used successfully in clinics. This means that a crystalline phase of TiO<sub>2</sub> is not a prerequisite for inducing hydroxyapatite formation. Uchida et al [41] have reported that the difference between amorphous and crystallized titanium oxide implied that not all Ti-OH groups, but certain types of Ti-OH groups in a specific structural arrangement, are effective in inducing apatite nucleation. The crucial part is how well structurally matched the interface between the organized hydroxylated surface and HA nuclei are, and also the surface charge.

When comparing hydroxylated 110 (anatase) and 0001 (HA) it is suggested that there are three important parts in matching their interface. (1) Hydrogen bond interaction; Ti-OH groups can form hydrogen bonds with OPO<sub>3</sub><sup>3-</sup> on the HA (0001) surface, and also with OH<sup>-</sup> on the HA (0001). (2) Crystal lattice matching, i.e., how the Ti-OH groups are arranged on the anatase (110) surface matching the HA (0001) (3) Stereochemical matching, which is the anatase OH<sup>-</sup> arrangement surrounding a Ca<sup>2+</sup> ion along the c-axis of HA, resulting in oriented nucleation [42].

The rutile (101) surface also has a lattice match with HA (0001) [41]. The nucleation of the crystallized species and their orientation tend to be determined more by stereochemical matching than lattice matching [31]. Anatase is speculated to have a higher bioactivity than rutile, due to a better lattice match with HA and a higher acidity, as well as lower surface ζ-potential, caused by a larger number of hydroxyl groups on the surface [43]. The degree of surface acidity at a given pH is the value of the surface ζ-potential. The surface ζ-potential is lower for a more acidic surface. It has been shown that deposition of HA on anatase, at pH 7.4, is faster than on rutile at the same pH, while a less negative ζ-potential will inhibit the HA nucleation [43]. Furthermore a rise in temperature and ion concentration increases the growth rate of HA [44].

Based on the theoretical considerations briefly outlined above, different chemical and physical methods have been used to improve the bioactivity of Ti based materials. In term of chemical methods, NaOH and HCl are typically used to treat the Ti surface [45]. A kind of sodium hydrogen titanate (Na<sub>x</sub>H<sub>2-x</sub>Ti<sub>3</sub>O<sub>7</sub>) is formed on the surface of titanium and its alloys after treatment in highly concentrated solutions of NaOH [45]. If this surface is subsequently treated with HCl solution, the sodium hydrogen titanate will transform into hydrogen titanate (H<sub>2</sub>Ti<sub>3</sub>O<sub>7</sub>) [45]. The Na<sup>+</sup> and H<sup>+</sup> ions could be released from the surface via exchanging with H<sub>3</sub>O<sup>+</sup> ions in the SBF to induce Ti-OH groups on the surface. However, the ability to induce hydroxyapatite formation after these treatments is relatively low. Only after such samples are further treated with heat to form rutile and anatase on the surface, can the ability of hydroxyapatite formation be improved significantly.

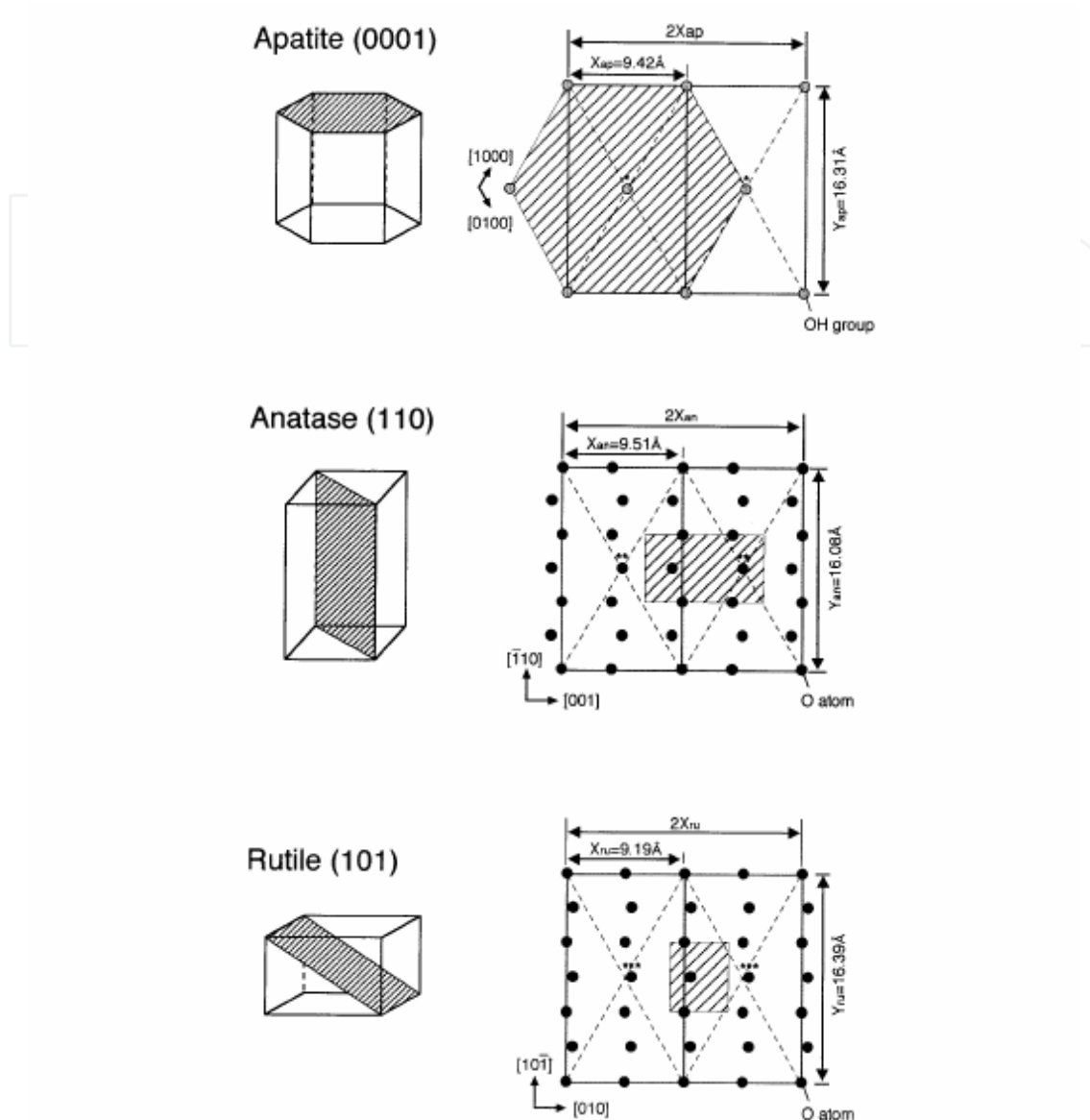


Fig. 3. Positions of hydroxyl group on (0001) plane in the hydroxyapatite crystal compared with those of oxygen on (110) plane of anatase and on (101) plane of rutile. [41]

Other methods to form or transform a crystalline titanium dioxide surface on Ti implants are important for the control of bioactivity, for examples, physical (e.g. physical vapour deposition) or heat treatment (the native amorphous surface transform into crystalline at temperature of about 300 degrees Celcius).

#### 4. Novel techniques of interface analysis

The study of the formation and properties of biomimetic coatings requires the use of analytical techniques that can provide nanoscale information about the crystallinity, morphology and chemical composition of the coatings. In this section we briefly describe a technique that has recently been used to obtain nanoscale information about the interface between apatites and bone.

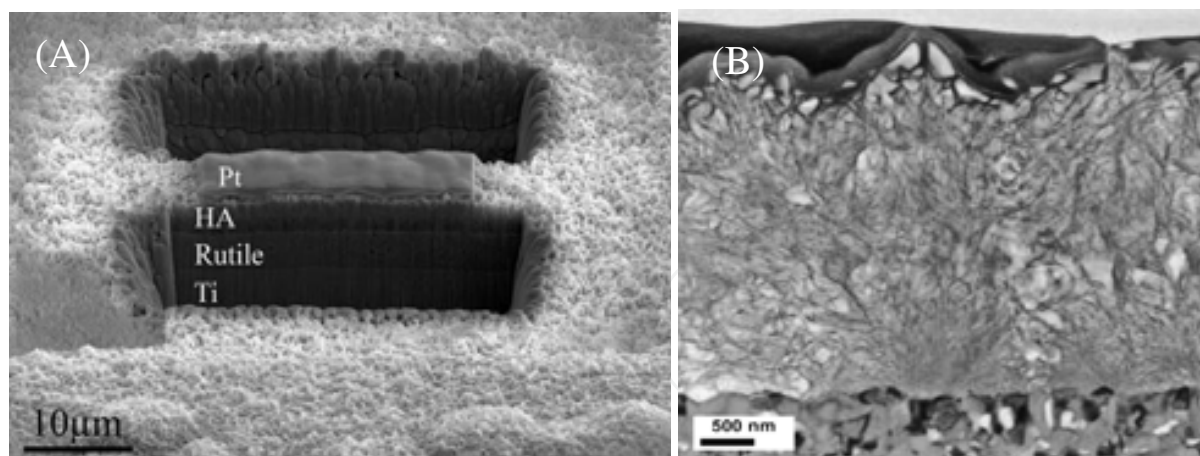


Fig. 4. (A) Preparation of a TEM sample using FIB,[46] (B) Cross-section TEM micrograph of the polycrystalline rutile  $\text{TiO}_2$  coated with HA.[30]

Focused ion beam (FIB) microscopy has previously been used extensively in the material science community, especially in the study of semiconductor devices in the microelectronics industry [48, 49]. The FIB system scans a beam of positively charged gallium ions over the sample, similar to the electron beam in the scanning electron microscope (SEM). The ions generate sputtered neutral atoms, secondary electrons, and secondary ions. The electrons or the positively charged ions can be used to form an image. The images taken within the FIB show a different contrast than the normal SEM images, which can give additional information. More significantly it is possible to increase the beam current of the primary ion beam and use the FIB as a fine-scale micro-machining tool. Production of transmission electron microscopy (TEM) samples using focused ion beam (FIB) microscopy provides the possibility of studying interfaces with precise control of the analysis site and the ability to mill the material down to electron transparency (**Fig. 4**). This technique facilitates studies of biomaterial-tissue and coating-implants interfaces [50, 51].

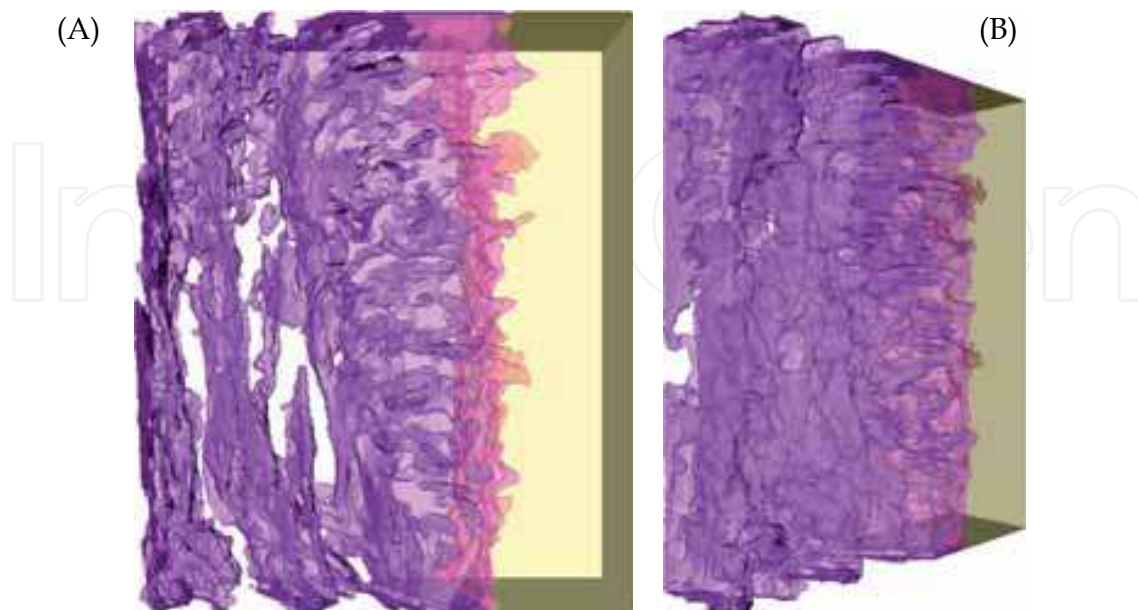


Fig. 5. Three dimensional reconstruction of the interface between human bone and a hydroxyapatite implant using Z-contrast electron tomography with FIB slice.[47]

Grandfield et al recently reported a three dimensional reconstruction of the interface between human bone and a hydroxyapatite implant using Z-contrast electron tomography with FIB slice (**Fig. 5**) [47]. Viewing this structure in three dimensions enabled observation of visualization of nanometre differences in the orientation of hydroxyapatite crystals precipitated on the implant surface in vivo versus those in the collagen matrix of bone. Insight into the morphology of biointerfaces is considerably enhanced with three-dimensional techniques.

## 5. Surface and interface analysis of biomimetic HA deposition on titanium oxide surfaces

Biomimetic HA deposition is mimicking the natural process of remineralization of hydroxyapatite, but without involving cellular and organic species. The surface chemistry of the substrate materials is an important factor for the coatings produced in these processes. The formation of a negatively charged surface composed with Ti-OH is a key step of inducing growth of new hydroxyapatite in a simulated body fluid, which for crystalline titanium dioxides can occur, as discussed in section 3.

No HA formation could be detected on sol-gel derived amorphous titanium oxide surfaces even after 14 days of soaking in SBF or PBS. But on both rutile and anatase HA forms readily in SBF or PBS solution. This implies that not all Ti-OH groups, but certain types of Ti-OH groups in a specific structural arrangement, are effective in inducing apatite nucleation [41, 52, 53] Nancollas explained that the surface tension of the metal oxides would influence the apatite nucleation. Uchida et al assumed the atomic arrangements in their crystal structures to be suitable for the epitaxy of apatite crystals. The good crystallographic matching is favorable to the apatite epitaxial growth along (0001) plane.

Engqvist et al has investigated some boundary conditions for HA formation on crystalline titanium oxide surfaces regarding influence of coating thickness, soaking time and soaking temperature [24]. The soaking temperature had an effect on the HA formation and

	1 h	1 day	1 week	4 weeks
4°C furnace	-	-	-	-
37°C furnace	-	HA	HA	HA
65°C furnace	-	HA	HA	HA

Table 4. HA growth for temperature versus time test matrix on oxidized rutile surfaces[24]

	1 h	1 day	1 week	4 weeks
4°C reference	-	-	-	-
37°C reference	-	-	-	-
65°C reference	-	-	HA	HA

Table 5. HA growth for temperature versus time test matrix on reference samples with native titanium oxide[24]

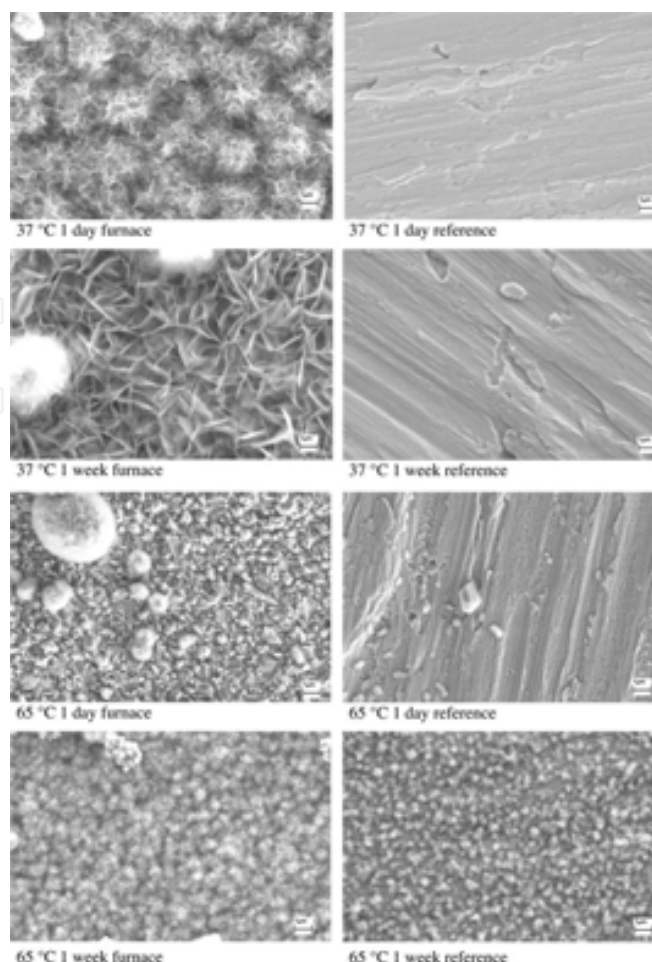


Fig. 6. SEM of HA formation at 37°C and 65°C on furnace treated samples and untreated references. None of the reference samples showed any HA growth except the 65°C immersed for 1 week [24].

growth on both rutile surfaces and native oxide on Ti substrates. Higher temperatures lead to more formation of HA. It was even possible, at 65°C, to grow HA on native titanium oxide by soaking in PBS. The coating quality was better for HA formed at 65°C compared to 37°C (**table 4 and 5, Fig. 6**).

Effects of titanium oxide PVD coating thickness (from 19 nm to 74 nm) on HA growth were also investigated [54]. All coatings were active, which is interesting from a surface modification point of view; it could well be sufficient to have very thin coatings to obtain the desired biological effect. One obvious benefit of thin coatings is the higher adhesion compared to thicker coatings. Thick coatings have higher internal stresses leading to higher probability of coating delamination. The PVD coated TiO<sub>2</sub> investigated was a graded bioactive coating, having a gradient by TiO<sub>2</sub> (~40nm), TiO<sub>x</sub> (~70nm) and the substrate, see **Fig. 7 and 8** [54]. The adhesion to the substrate was above 1 GPa.

Because biomimetic HA coating is deposited from a supersaturated phosphate buffer solution, it shows a porous structure. So the internal strength of this coating is expected to be low, as compared to coatings prepared by sputtering methods. Forsgren et al used a scratch test to assess the adhesion of the biomimetic HA coatings [30]. This is a well established method to provide a measure of the coating-to-substrate adhesion and was found to be a useful method to test the thin HA coatings deposited on the bioactive surfaces. The critical pressure of the layer was estimated to be  $2.4 \pm 0.1$  GPa [30].

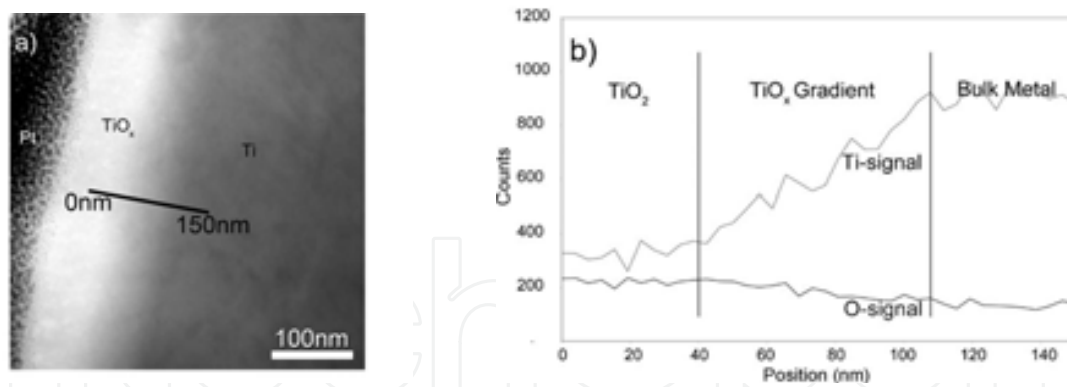


Fig. 7. (a) STEM image showing the titanium oxide layer in cross-section. The coating features are marked in the image and (b) the corresponding line profiles of Ti and oxygen over the marked line from 0 nm to 150 nm as obtained by EDS are displayed.[54]

In order to ensure coating sterility and to increase the adhesion, biomimetic hydroxyapatite (HA) coatings on titanium oxide have been heat-treated at 600 and 800°C for one hour [46]. The 600 °C heat treatment of the HA coating changed its morphology, increased its grain size and also increased the porosity. At 800 °C the coating was completely transformed to  $\beta$ -TCP according to XRD, see Fig.9. Fig. 10 shows that the HA crystal size increased after heat treatment, but the morphology was still porous.

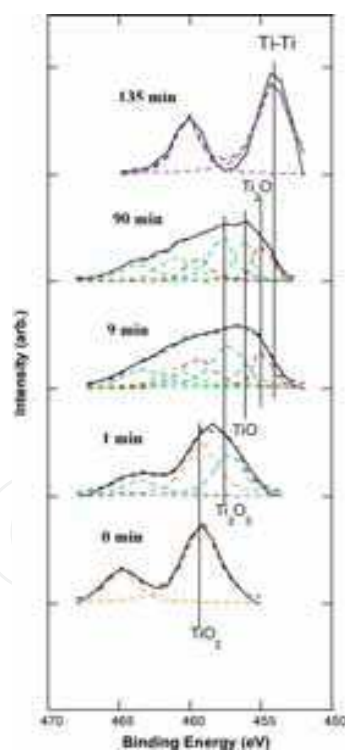


Fig. 8. XPS Ti 2p spectra (solid line) showing peak shift in titanium oxide after sputtering through the coating at the displayed times. Incorporated in the figures are curve fits, assuming Lorenzian-Gaussian Ti 2p photo peaks, to literature values [23] of binding energies for various Ti containing phases (broken lines). Vertical solid lines, indicating the binding energy of the Ti 2p<sub>3/2</sub> peak, for TiO<sub>2</sub>, Ti<sub>2</sub>O<sub>3</sub>, TiO, Ti<sub>2</sub>O and pure Ti are also included in the figure.[54]

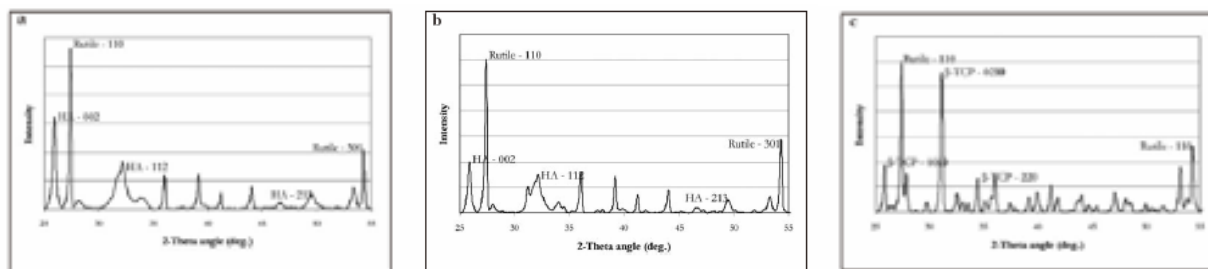
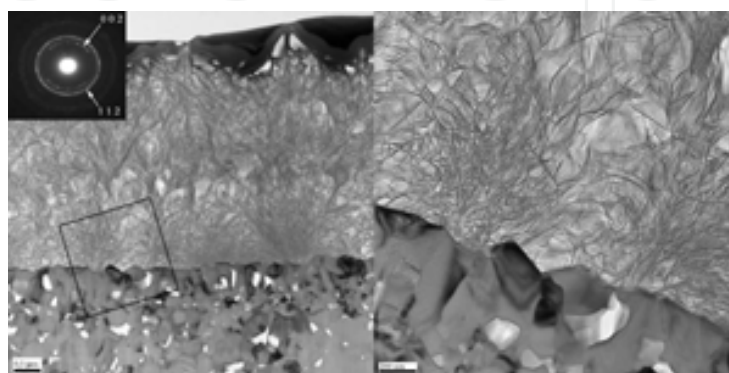
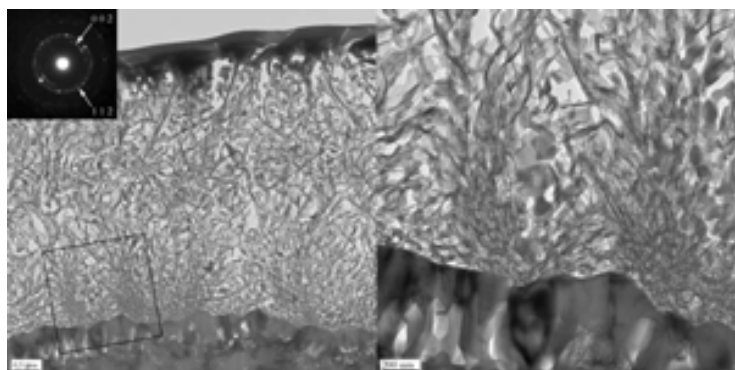


Fig. 9. XRD of biomimetic HA coating on rutile. The strongest diffraction peaks are indexed. (a) Untreated HA, (b) HA heat treated at 600 °C, (c) HA heat treated at 800 °C. [46]



(A)



(B)

Fig. 10. TEM image of HA formed on rutile (A) and heat treated at 600 °C (B). The square shows where the right micrograph was acquired. [46]

### Fundamental studies of HA growth on titanium oxide

Uchida et al showed that for certain crystallographic planes in the two ordered  $\text{TiO}_2$  structures rutile and anatase the oxygen position match well with the hydroxyl groups in hydroxyapatite [41]. This could provide an answer why hydroxyapatite will not grow readily on amorphous  $\text{TiO}_2$ , since here the oxygen positions are not ordered. Epitaxial nucleation of hydroxyapatite on rutile is expected to occur based on the two-dimensional similarity of the two structures. Muller et al. studied the orientation of crystals in a hydroxylapatite film grown on titanium metal with a coating layer of  $\text{TiH}_{2-x}$  [55]. They found from electron diffraction that the crystallites in the film were preferentially oriented with the c axis of the hydroxyapatite directed out from the surface. The preferential orientation was

limited to the outer parts of the hydroxyapatite precipitate. Hydroxyapatite crystals are plate-shaped with [001] HA normal to the plane of the plate and [100] HA within that plane [56]. When precipitated, the plates are oriented perpendicular to the substrate surface, so that the fast-growing [100] HA direction is projected outward.

Engqvist et al also reported experimental observations of early growth and growth of hydroxyapatite on single-crystal rutile substrates (100), (001), and (110) [57]. The specific crystal faces of rutile were used to study if hydroxyapatite grows differently depending on the crystal surface of rutile, and also to investigate the previously presented hypothesis of epitaxial growth of hydroxyapatite on rutile.

**Table 6** shows the atomic concentrations for detected elements for an immersion series with the (110) surface. The data shows a continuous increase of the Ca and P concentrations, as well as Ca/P ratio, with immersion time. The Ca/P ratio is in all cases far below the expected for hydroxyapatite (nominal Ca/P ratio of 1.67).

	(110) ref	(110) 10 min	(110) 1 h	(110) 24 h	(001) 24 h
Ti	20.70	22.00	20.10	19.41	18.67
O	51.26	56.39	56.83	56.00	55.28
C	25.36	20.23	21.39	21.99	23.40
N	1.21	0.97	1.07	1.50	1.38
Si	1.04	0.00	0.00	0.00	0.00
Ca	0.00	0.03	0.08	0.20	0.29
P	0.00	0.41	0.53	0.91	1.01
Ca/P	n.a.	0.06	0.14	0.22	0.28

Values are mean of two measurement areas on each sample

Table 6. Relative concentrations (at.%) of elements detected in XPS analyses. Also shown are the Ca/P ratios[57]

Comparison between the (110) and (001) surfaces after 24 immersion shows higher Ca and P values for the latter. The relative intensities of the calcium and phosphate signals, as measured by time-of-flight secondary ion mass spectrometry (ToF-SIMS, see **Fig. 11**), varied for the different crystalline directions and PBS immersion times. The adsorption of calcium and phosphate ions was faster on the (001) and (100) surfaces than on the (110) surface. The measured Ca/P ratios were in all cases far below that of hydroxyapatite and other calcium phosphates, showing that no crystal formation had taken place at the surfaces after the studied immersion times.

Hydroxyapatite grown on different surfaces has fundamentally different appearances (**Fig. 12**). On the (001) surface of rutile the hydroxyapatite crystallites grow as a dense layer, with the platelike crystallites growing side by side, **Fig. 12a**. On the fast growing direction (100) HA points out from the surface. This was similar to the growth in the polycrystalline rutile, but in contrast to the growth on the (110) surface. On the (110) surface the crystallites grew in bundles. Spheres made up of several hydroxyapatite crystals were formed on the substrate surface, see **Fig. 12c**. Precipitates that had been stopped at an early stage were also studied by SEM. On the (001) surface it could be seen that underneath every upward-projecting crystallite there was another crystal lying flat on the surface, **Fig. 12b**. This could not be seen in early stages of growth on the (110) surface. Here the crystallites immediately formed spherical bundles, see **Fig. 12d**. At early stages of precipitation on the (100) surface, few and randomly oriented crystallites without the distinct plate-like shape were seen. At later stages, however, dense layers of upright crystallites were seen, **Fig. 12e and f**.

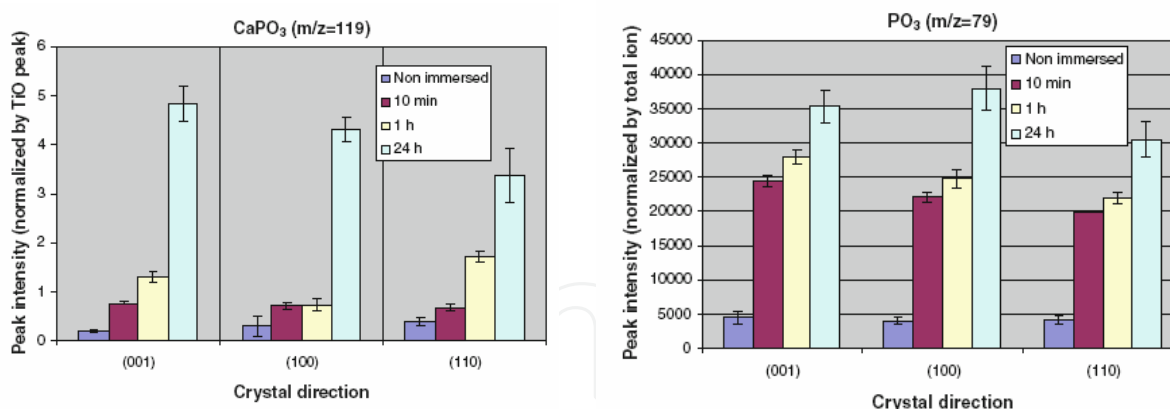


Fig. 11. Relative peak intensities CaPO<sub>3</sub><sup>+</sup> and PO<sub>3</sub><sup>-</sup> for different crystal surfaces and PBS immersion times. The CaPO<sub>3</sub><sup>+</sup> Peak intensities are normalized against the TiO<sup>+</sup> signal from TiO<sub>2</sub> and the PO<sub>3</sub><sup>-</sup> signal is normalized against total ion intensity. Values shown are mean ± standard deviation for three measurement areas on each sample.[57]

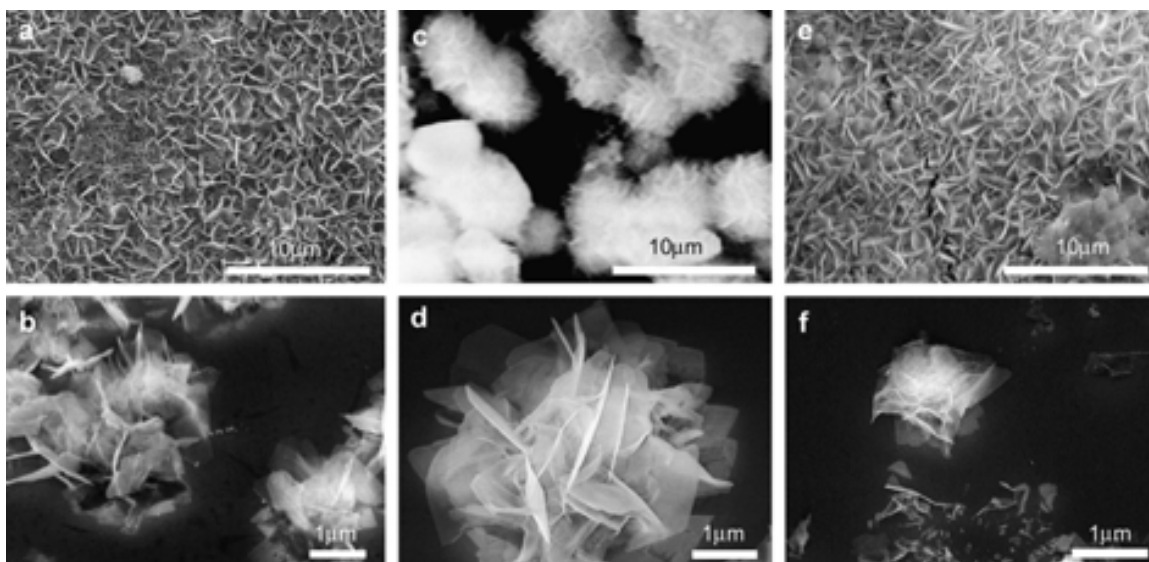


Fig. 12. Precipitation of hydroxylapatite on single-crystal substrates. (a), (c) and (e) show late stages of the precipitation process on the (001), (110) and (100) rutile surfaces, respectively. In (a) and (e) dense films of upright crystallites have formed, while in (c) the crystallites are bundled in ball-like aggregates. (b), (d) and (f) show early stages. On the (001) surface, a crystal is often seen lying flat beneath later precipitated crystals. This is not seen on the other surfaces.[31]

A good adhesion while was noted between rutile and HA at the (001) and (110) surfaces of rutile and for polycrystalline rutile, substrate-hydroxyapatite contact seemed poor at the (100) surface (**Fig. 13**). Across the whole nucleation interface in the TEM sample, the first 20 nm of the hydroxyapatite growth had the same orientation. The fast Fourier transform analysis (FFT) of the hydroxyapatite part of the micrograph (**Fig. 14**) indicated that the detected planes were (112) and (202). Thus, the [001] HA axis, which is parallel to the c axis in hydroxyapatite, is in this case oriented along the substrate surface and 11° off from the [001] rutile direction; the [100] HA was rotated about 14° away from the normal to the rutile surface. The hydroxyapatite crystals grow with their (001) HA direction along the (110)

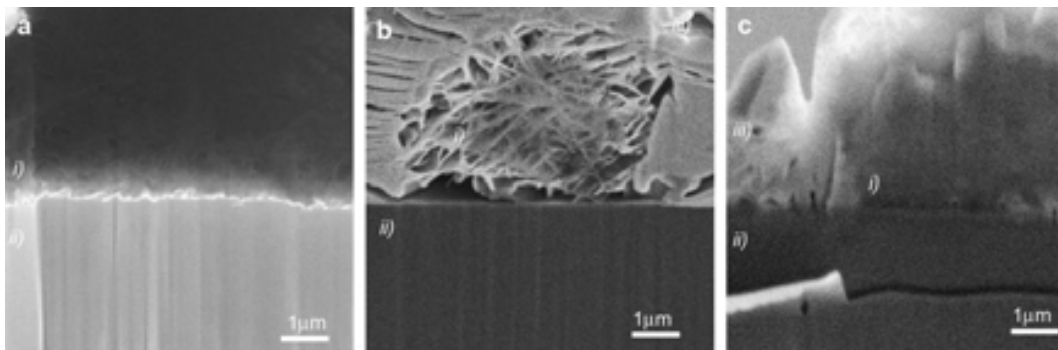


Fig. 13. SEM images recorded during the TEM sample preparation in the FIB. In the pictures (i) depicts hydroxylapatite, (ii) rutile, and (iii) the protective Pt layer deposited during the sample preparation. A solid interface is produced between the PVD-produced polycrystalline rutile surface and hydroxylapatite (a), the 001 surface and hydroxylapatite (c), and the (110) surface and hydroxylapatite (not shown). On the other hand, the interface between the (100) surface and hydroxylapatite (b) is porous and lacks good adhesion.[31]

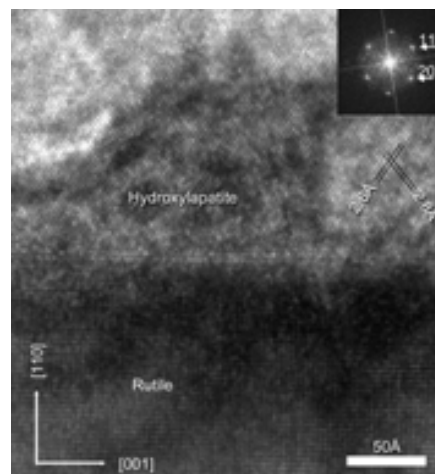


Fig. 14. On the (110) rutile surface, looking along  $[1-10]$ , a 20 nm layer with the same orientation of hydroxylapatite has grown over the whole nucleation surface. From the inserted FFT, taken from that layer, the 112HA and 202HA are seen, and it can be concluded that  $[001]$  HA is oriented parallel to the substrate surface.[31]

rutile surface is an observation that seems general (**Fig. 15a and b**), which also constitute an image of the interface on the (110) surface, but instead recorded along the rutile zone axis  $[001]$ .

This micrograph was taken at a lower magnification, allowing a large number of crystals to be included in the FFT calculation in order to obtain better statistics in the analysis. The FFT analysis reveals the (100) HA and equivalent to be oriented out from the surface, and thus the  $c$  axis of hydroxylapatite to be oriented along the rutile crystal face. However, as can be seen by the FFT analysis, an acceptance angle of the spread of the spots representing the direction of (100) HA is present, but no indication of ordering of (100) HA along the surface plane or of (001) HA growing out from the surface. On the (001) surface hydroxyapatite grew in another preferential direction. Contrary to the situation on the (110) surface, the FFT analysis here indicated that (100) HA and equivalent reflections are oriented along the surface (**Fig. 15c and d**). Furthermore, spots representing the (001) HA direction indicate the hydroxyapatite  $c$  axis to be oriented normal to the substrate surface.

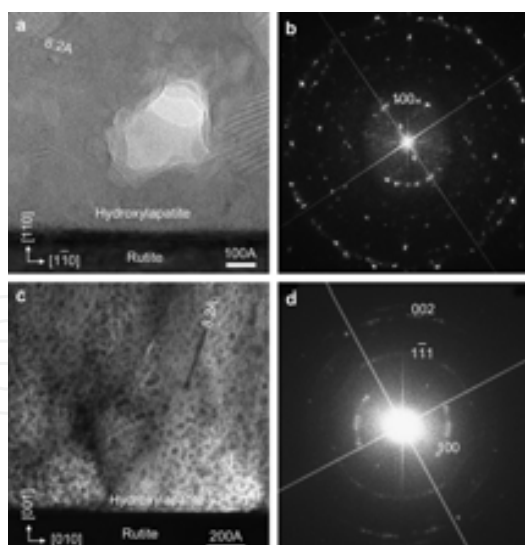


Fig. 15. (a) Micrograph recorded from the interface between hydroxyapatite and rutile (110), and (b) the corresponding FFT. The lattice fringes corresponding to the 100 spacing are indicated in the figure. In (b) it can be seen that the 100 reflection preferentially, with an acceptance angle, orders normal to the substrate surface. (c) Micrograph recorded from the interface between hydroxyapatite and rutile (001) and (d) the corresponding FFT. Judging from the FFT, the hydroxyapatite crystallites align with the c axis normal to the substrate surface, but with a directional spread of about  $\pm 25^\circ$ . [31]

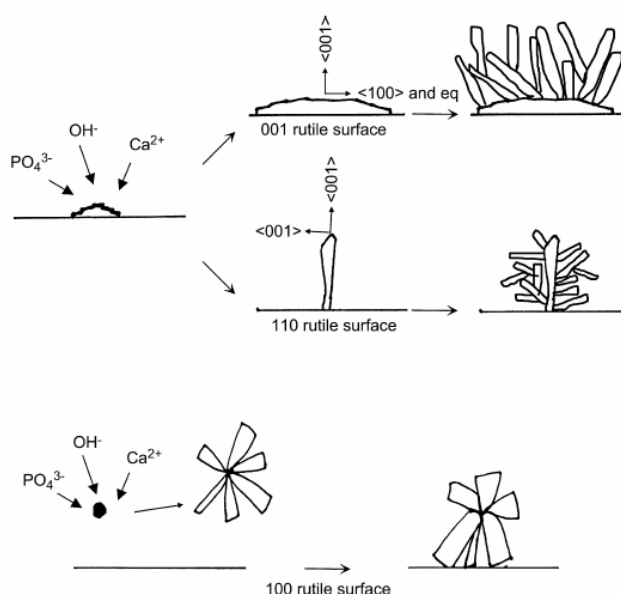


Fig. 16. Possible scenarios for the precipitation of hydroxyapatite on different rutile surfaces. [31]

Similar analysis of images taken further up in the hydroxyapatite layer, i.e., not at the interface, shows random orientation of the crystallites. Preferred orientation of the crystallites seems to be limited to the first few hundred nanometres. This explains why XRD does not reveal preferred orientation. Since the sampling volume is relatively large using this technique, the scattering from the immediate interface plays a minor role.

A possible scenario for the process of hydroxyapatite precipitation of hydroxyapatite on different rutile surfaces is shown in **Fig. 16**. At the rutile (001) surface, the hydroxyapatite nucleation seed orients so that further crystallization can proceed along the surface. At the (110) surface, the seed will nucleate so that the fast-growing directions of hydroxyapatite project out from the surface. Twin formation and dislocations in the basal layer make nucleation of additional crystals possible. The poor adhesion at the (100) rutile surface may arise if crystallites suspended in the solution form bundles that later attach to the surface. As the results, the specific orientation of the hydroxyapatite precipitate nucleus on the (001) surface leads to faster coverage of this surface compared to the (110) and (100) rutile surfaces. The preferred orientation of the precipitate is limited to the first few hundred nanometers, and the immediate interface indicated random orientation.

## 6. Growth of biomimetic ion doped HA on titanium oxide surfaces

Hydroxyapatite in bone is a multi-substituted calcium phosphate, including traces of  $\text{CO}_3^{2-}$ ,  $\text{F}^-$ ,  $\text{Mg}^{2+}$ ,  $\text{Sr}^{2+}$ ,  $\text{Si}^{4+}$  etc [8]. Anions can be incorporated into the sites of  $\text{OH}^-$  (type A) and  $\text{PO}_4^{3-}$  (type B) [58], and cations can be incorporated into the sites  $\text{Ca}^{2+}$  I and  $\text{Ca}^{2+}$  II [59]. These ionic substitutions play an important role in bone formation. There has been a significant research interest on the effects of  $\text{CO}_3^{2-}$ ,  $\text{F}^-$ ,  $\text{Si}^{4+}$  ions on the bioactivity of hydroxyapatite [60-63]. These ion substitutions not only change the composition, solubility and crystallinity of HA but also are important in cell proliferation, collagen synthesis, nuclei acid synthesis, bone development, and have pharmaceutical effects on bone regeneration. For example, strontium ranelate can reduce the incidence of fracture in osteoporotic patients.[64] The low dose administration of silicon and strontium could increase bone mass and strength by inhibiting bone resorption and augmenting bone formation.[65, 66] A local release of these trace elements at low dose is good for bone regeneration with a low drug usage compared to oral administration and injection. Silicon can increase the bone mineralization rate and enhance the osteoblast proliferation, differentiation and collagen production [62]. Fluoride, which is good for teeth, can stabilize apatite and also stimulate the osteoblast activity [61, 67]. Magnesium has been found in high concentrations in bone and cartilage tissue during the initial phases of osteogenesis, and to cause the acceleration of the nucleation kinetics of hydroxyapatite and to inhibit its crystallization process. Zn is known to be an essential trace element. It is important in the normal growth and development of the skeletal system and its deficiency is associated with a decrease in bone density [68]. Zn inhibits osteoclast differentiation and promotes osteoblast activity [69], and thus promotes bone formation.

Although biological hydroxyapatite has been used as coatings on metallic implants, there is room for improvement of this biomimetic coating in order to strengthen the implant and bone bonding and to have a stronger positive effect on new bone formation. Except for that, these ions could play their pharmaceutical functions at the same time.

Biomimetic methods for coating deposition involve mild conditions similar to those characteristic of biological environments, and allow deposition of CaP coatings on many different objects, such as metal surfaces, sponges, cements and fixation rods [70]. This is suitable for preparing the biomimetic ion substituted HA (iHA) on titanium oxide surfaces. At present, different kinds of biomimetic iHA coatings have been reported, such as  $\text{CO}_3^{2-}$ ,  $\text{F}^-$ ,  $\text{Mg}^{2+}$ ,  $\text{Zn}^{2+}$ ,  $\text{Sr}^{2+}$   $\text{Mn}^{2+}$  and  $\text{Si}^{4+}$ . Here we will focus on the iHA coatings on titanium oxides surfaces.

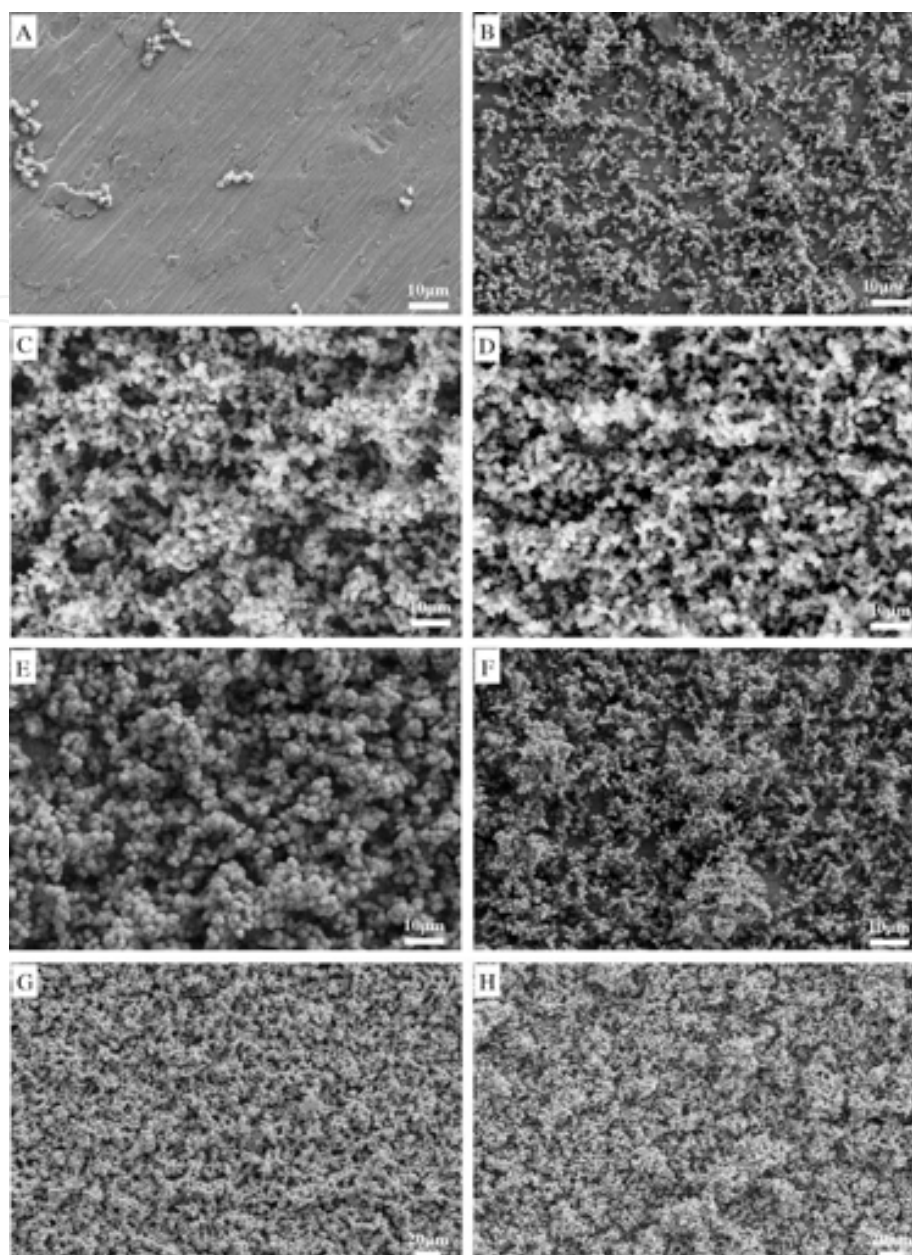


Fig. 17. SEM images of the PVD-treated titanium surface after soaking in Sr-PBS for 1 and 2 weeks. (A) 0.06 mM at 37°C for 1 week, (B) 0.6 mM at 37°C for 1 week, (C) 0.06 mM at 37°C for 2 weeks, (D) 0.6 mM at 37°C for 2 weeks, (E) 0.06 mM at 60°C for 1 week, (F) 0.6 mM at 60°C for 1 week, (G) 0.06 mM at 60°C for 2 weeks and (H) 0.6 mM at 60°C for 2 weeks.[25]

Biomimetic strontium substituted apatite coating on crystallized titanium oxide surface has been studied regarding its morphology, crystallinity, surface chemistry and composition as functions of soaking temperature and time in phosphate buffer solutions with different Sr ion concentration [25]. The increase of soaking temperature and time improved the formation rate and crystallinity of SrHA coatings, but could not greatly change the strontium content in the coating, whereas the concentration of strontium ion in the soaking medium influenced the surface composition. **Fig. 17** shows the changes of surface morphologies of SrHA coatings as functions of the concentration of Sr ion, soaking temperature and time. However, the morphology of SrHA crystals could be changed by the

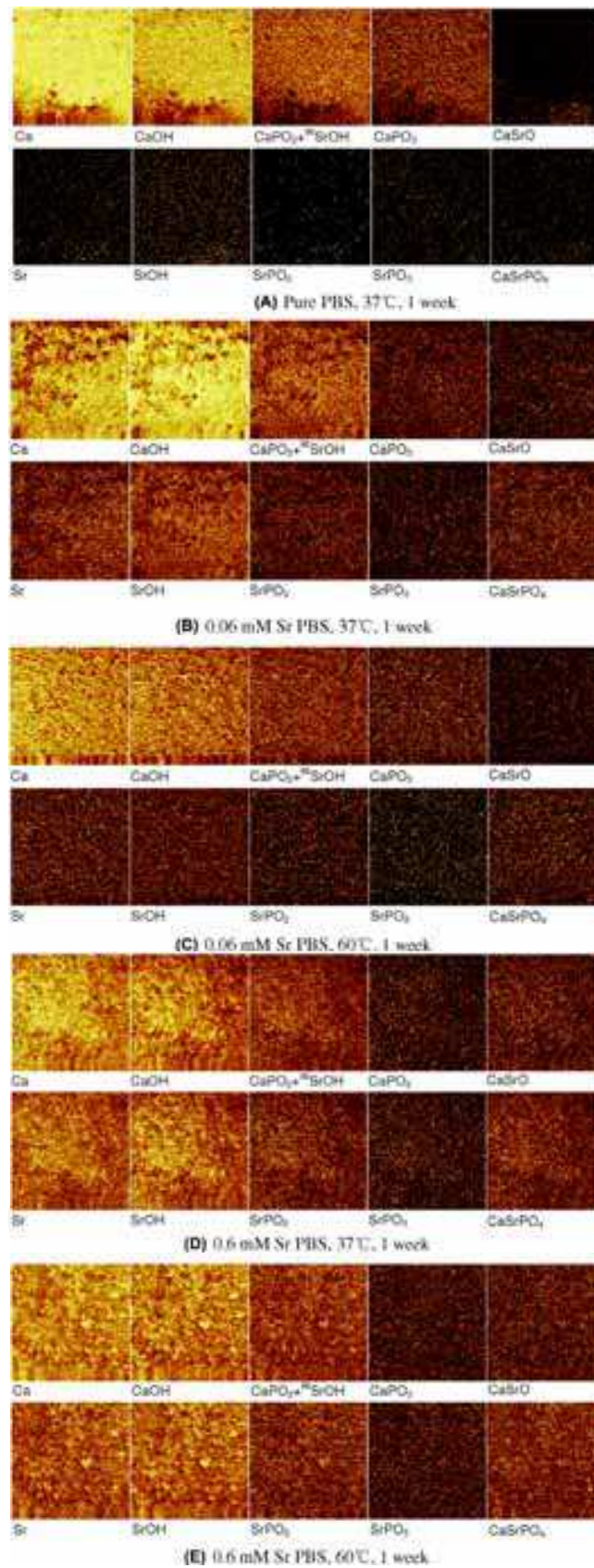
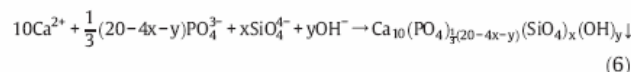


Fig. 18. TOF-SIMS ion images of the Sr-substituted apatite/titanium dioxide coating on titanium oxide [25]

soaking medium from plate-like to sphere-like [25]. Ion images obtained from ToF-SIMS analyses show homogeneous Ca and Sr distributions, indicating co-localization of the Ca and Sr ions (**Fig. 18**).

Silicon doped hydroxyapatite coating deposited on titanium oxide has been reported by Zhang and Xia et al [71, 72]. Similar morphology with biomimetic hydroxyapatite has been observed (**Fig. 19**). Cracks are also observed due to the dehydration shrinkage. The coating thickness was 5-10 $\mu$ m with a shear strength in the order of  $\sim$ 16MPa. The chemical reactions in the solution could be illustrated as following [71]:



Silicon was confirmed to exist in the form of  $\text{SiO}_4^{4-}$  groups in biomimetic SiHA coating.

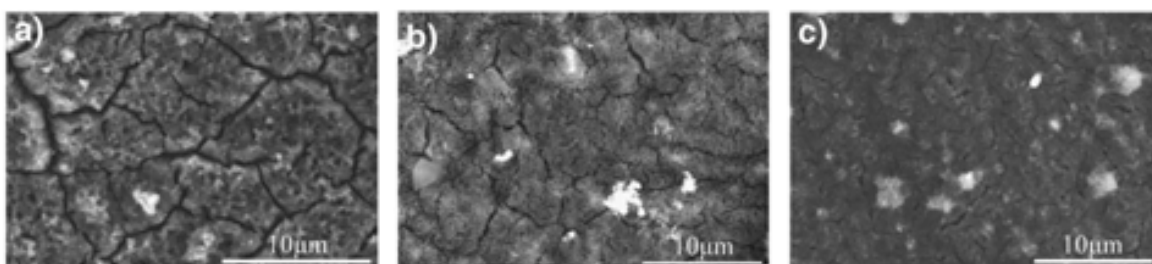


Fig. 19. SEM surface micrographs of biomimetic SiHA coatings obtained from different silicon modified Hank's balanced salt solution, (a) 1mM; (b) 5mM; (c) 100mM.[71]

## 6. Biological response of biomimetic HA coatings

Calcium phosphate based coatings on titanium implants are now accepted to be suitable for enhancing bone formation around implants, to contribute to cementless fixation and thus to improve clinical success at an early stage after implantation [70]. Narayanan and Kim et al summarized the interface reactions as following five steps [70].

1. Dissolution of calcium phosphate based coatings,
2. Re-precipitation of apatite,
3. Ion exchange accompanied by absorption and incorporation of biological molecules,
4. Cell attachment, proliferation and differentiation,
5. Extracellular matrix formation and mineralization.

The dissolution of HA coating is a key step to induce the precipitation of bone-like apatite on the implant surface. Because the biomimetic hydroxyapatite coatings have a low degree of crystallinity and porous structure, their solubility is higher than the for dense hydroxyapatite coatings deposited with other methods. That is bone expected to be

beneficial to early bone formation. Otherwise, rough and porous surfaces could stimulate cell attachment and formation of extra-cellular matrix [73].

The biological benefits/effects of biomimetic HA [63, 74-76] and the possibilities to use them as coatings on titanium implants for improving the biological responses have been reported. However, only a few of the developed ion-substituted and/or ion doped hydroxyapatite coatings have been tested in vitro and/or in vivo, and the improvement of the biological response due to ion substitution is thus still just a hypothesis [20, 27, 77-79]. For biomimetic SiHA coatings on heat treated titanium, Zhang et al reported higher cell proliferation on this type of deposition, and the bone ingrowth rate (BIR) was not only significantly higher than for uncoated titanium, but also significantly higher than for biomimetic hydroxyapatite coated titanium [79].

## 7. Conclusions

Crystallized titanium oxides induce bone-like hydroxyapatite on its surface, which can be hypothesized as an important early step for osseointegration. The understanding of mechanisms behind biomimetic HA depositions on titanium oxide surfaces could therefore contribute to increased understanding the mechanism of the osseointegration, and also provide a scientific basis for design and control of biomimetic layers for medical applications. Deposition of biomimetic hydroxyapatite on titanium oxide surfaces, acting as a bonding layer to the bone, might improve the bone-bonding ability and enhance the biological responses to bone anchored implants.

## 8. References

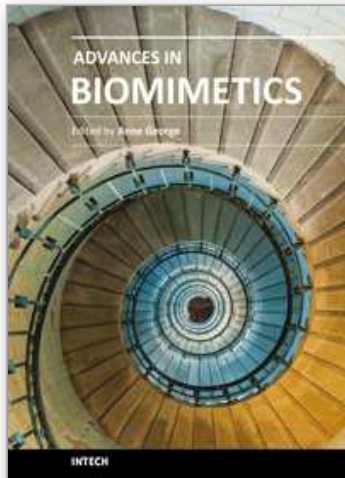
- [1] Ellingsen JE, Lyngstadaas SP. Bio-implant interface: improving biomaterials and tissue reactions, CRC Press, USA.
- [2] Zhou W, Zong X, Wu X, Yuan L, Shu Q, Xia Y. Plasmacontrolled nanocrystallinity and phase composition of TiO<sub>2</sub>: a smart way to enhance biomimetic response J Biomed Mat Res 2007;81A:453-464.
- [3] Lausmaa J. Surface spectroscopic characterization of titanium implant materials. J Electron Spectr Related Phenom 1996;81:343-361.
- [4] Ellingsen J. A study on the mechanism of protein adsorption to TiO<sub>2</sub>. Biomaterials 1991;12:593-596.
- [5] Kido H, Saha S. Effect of HA coating on the long-term survival of dental implant: a review of the literature. J Long Term Eff Med Implants 1996;6(2):119-133.
- [6] Hench L. Bioceramics: From concept to clinic. J Am Ceram Soc 1991;74:1487-1510.
- [7] Boanini E, Gazzano M, Bigi A. Ionic substitutions in calcium phosphates synthesized at low temperature. Acta Biomater 2009; 6(6):1882-1894.
- [8] Dorozhkin SV, Epple M. Biological and medical significance of calcium phosphates. Angew Chem Int Ed Engl 2002;41(17):3130-3146.
- [9] Vallet-Regí M. Ceramics for medical applications. J Chem Soc, Dalton Trans 2001:97-108.
- [10] Kim H, Koh Y, Li L, Lee S, Kim H. Hydroxyapatite coating on titanium substrate with titania buffer layer processed by sol-gel method. Biomaterials 2004;25:2533-2538.
- [11] Montenero A, Gnappi G, Ferrari F, Cesari M, Salvioli E, Mattogno L, Kaciulis S, Fini M. Sol-gel derived hydroxyapatite coatings on titanium substrate. J Mater Sci 2000;35:2791-2797.

- [12] Thian E, Khor K, Loh N, Tor S. Processing of HA-coated Ti-6Al-4V by a ceramic slurry approach: An in vitro study. *Biomaterials* 2001;22:1225-1232.
- [13] Gledhill H, Turner I, Doyle C. Direct morphological comparison of vacuum plasma sprayed and detonation gun sprayed hydroxyapatite coatings. *Biomaterials* 1999;20:315-322.
- [14] Inagaki M, Hozumi A, Okudera H, Yokogawa Y, Kameyama T. Improvement of chemical resistance of apatite/titanium composite coatings deposited by RF plasma spraying: Surface modification by chemical vapor deposition. *Thin Solid Films* 2001;382:69-73.
- [15] Massaro C, Baker M, Cosentino F, Ramires P, Klose S, Milella E. Surface and biological evaluation of hydroxyapatite-based coatings on titanium deposited by different techniques. *J Biomed Mater Res* 2001;58:651-657.
- [16] Cleries L, Fernandez-Pradas J, Morenza J. Bone growth on and resorption of calcium phosphate coatings obtained by pulsed laser deposition. *J Biomed Mater Res* 2000;49:43-52.
- [17] Fernandez-Pradas J, Cleries L, Sardin G, Morenza J. Hydroxyapatite coatings grown by pulsed laser deposition with a beam of 355 nm wavelength. *J Mater Res* 1999;14:4715-4719.
- [18] Yen S, Lin C. Cathodic reactions of electrolytic hydroxyapatite coating on pure titanium. *Mater ChemPhys* 2002;77:70-76.
- [19] Kameyama T. Hybrid bioceramics with metals and polymers for better biomaterials. *Bull Mater Sci* 1999;22:641-646.
- [20] Jalota S, Bharduri S, Tas A. Using a synthetic body fluid (SBF) solution of 27 mM HCO<sub>3</sub><sup>-</sup> to make bone substitutes more osteointegrative. *Mater Sci Eng C* 2008;28:129-140.
- [21] Kokubo T, Kushitani H, Sakka S, Kitsugi T, Yamamuro T. Solutions able to reproduce in vivo surface-structure change in bioactive glass-ceramic A-W. *J Biomed Mater Res* 1990;24:721-734.
- [22] Pasinli A, Yuksel M, Celik E, Sener S, Tas AC. A new approach in biomimetic synthesis of calcium phosphate coatings using lactic acid-Na lactate buffered body fluid solution. *Acta Biomaterialia* 2010;6:2282-2288.
- [23] Kokubo T, Takadama H. How useful is SBF in predicting in vivo bone bioactivity? *Biomaterials* 2006;27:2907-2915.
- [24] Lindgren M, Astrand M, Wiklund U, Engqvist H. Investigation of boundary conditions for biomimetic HA deposition on titanium oxide surfaces. *J Mater Sci Mater Med* 2009;20(7):1401-1408.
- [25] Xia W, Lindahl C, Lausmaa J, Borchardt P, Ballo A, Thomsen P, Engqvist H. Biomaterialized strontium-substituted apatite/titanium dioxide coating on titanium surfaces. *Acta Biomater* 2010;6(4):1591-1600.
- [26] Elliot JC. *Structural and chemistry of the apatites and other calcium orthophosphates*. Amsterdam, Elsevier 1994.
- [27] Boanini E, Gazzano M, Bigi A. Ionic substitutions in calcium phosphates synthesized at low temperature. *Acta Biomater* 2010;6(6):1882-1894.
- [28] Onuma K, Ito A. Cluster growth for hydroxyapatite. *Chem Mater* 1998;10:3346-3351.
- [29] Gamble J. *Chemical anatomy, physiology and pathology of extracellular fluid*. Cambridge, MA: Harvard University Press, 1967.

- [30] Forsgren J, Svahn F, Jarmar T, Engqvist H. Formation and adhesion of biomimetic hydroxyapatite deposited on titanium substrates. *Acta Biomater* 2007 Nov;3(6):980-984.
- [31] Lindberg F, Heinrichs J, Ericson F, Thomsen P, Engqvist H. Hydroxylapatite growth on single-crystal rutile substrates. *Biomaterials* 2008;29(23):3317-3323.
- [32] Barrere F, van Blitterswijk CA, de Groot K, Layrolle P. Influence of ionic strength and carbonate on the Ca-P coating formation from SBFx5 solution. *Biomaterials* 2002;23(9):1921-1930.
- [33] Tas AC, Bhaduri SB. Rapid coating of Ti6Al4V at room temperature with a calcium phosphate solution similar to 10× simulated body fluid. *J Mater Res* 2004;19:2742-2749.
- [34] Hanks JH, Wallace RE. Relation of oxygen and temperature in the preservation of tissues by refrigeration. *Proc Soc Exp Biol Med* 1949;71:196-200.
- [35] Ottaviani MF, Ceresa EM, Visca M. Cation Adsorption at the TiO<sub>2</sub>-Water Interface. *J Colloid Interf Sci* 1985;108:114-122.
- [36] Poznyak SK, Pergushov VI, Kokorin AI, Kulak AI, Scapfer CW. Structure and Electrochemical Properties of Species Formed as a Result of Cu(II) Ion Adsorption onto TiO<sub>2</sub> Nanoparticles. *J Phys Chem B* 1999;103:1308-1315.
- [37] Malati MA, Smith AE. The Adsorption of the Alkaline Earth Cations on Titanium Dioxide. *Powder Technol* 1979;22:279-282.
- [38] Kosmulski M. The significance of the difference in zero charge between rutile and anatase. *Adv Colloid Interfac* 2002;99:255-264.
- [39] Vassileva E, Proinova I, Hadjiivanov K. Solid-Phase Extraction of Heavy Metal Ions on a High Surface Area Titanium Dioxide (Anatase). *Analyst* 1996;121:607-612.
- [40] Winkler J, Marme S. Titania as a Sorbent in Normal-Phase Liquid Chromatography. *J Chromatogr A* 2000;888:51-62.
- [41] Uchida M, Kim HM, Kokubo T, Fujibayashi S, Nakamura T. Structural dependence of apatite formation on titania gels in a simulated body fluid. *J Biomed Mater Res A* 2003;64(1):164-170.
- [42] Mao C, Li H, Cui F, Ma C, Feng Q. Oriented growth of phosphates on polycrystalline titanium in a process mimicking biomineralization. *J Cryst Growth* 1999;206:308-321.
- [43] Svetina M, Colombi L, Sbaizero O, Meriani S, A. D. Deposition of calcium ions on rutile (110): A first-principles investigation. *Acta Mater* 2001;49:2169-2177.
- [44] Kim H. Ceramic bioactivity and related biomimetic strategy *Current Opinion in Solid State and Materials Science* 2003;7(4-5):289-299.
- [45] Kokubo T. *Bioceramics and their clinical applications*: CRC, 2008.
- [46] Forsgren J, Svahn F, Jarmar T, Engqvist H. Structural change of biomimetic hydroxyapatite coatings due to heat treatment. *J Appl Biomater Biomech* 2007;5(1):23-27.
- [47] Grandfield K, McNally E, Palmquist A, Botton G, Thomsen P, Engqvist H. Visualizing biointerfaces in three dimensions: electron tomography of the bone-hydroxyapatite interface *J R Soc Interface* 2010;7:1497-1501.
- [48] Phaneuf M. Applications of focused ion beam microscopy to material science specimens *Micron* 1999;30:277-288.

- [49] Giannuzzi L, Stevie F. Introduction to Focused Ion Beams: Theory, Instrumentation, Applications and Practice. Boston: Kluwer Academic, 2004.
- [50] Engqvist H, Botton GA, Couillard M, Mohammadi S, Malmström J, Emanuelsson L, Hermansson L, Phaneuf MW, Thomsen P. A novel tool for high-resolution transmission electron microscopy of intact interfaces between bone and metallic implants *J Biomed Mater Res* 2006;78:20-24.
- [51] Forsgren J, Svahn F, Jarmar T, Engqvist H. Formation and adhesion of biomimetic hydroxyapatite deposited on titanium substrates. *Acta Biomaterialia* 2007;3:980-984.
- [52] Wu W, Nancollas G. Kinetics of Heterogeneous nucleation of calcium phosphates on anatase and rutile Surface. *J Colloid Inter Sci* 1998;199:206-211.
- [53] Nancollas G, Wu W, Tang R. The Mechanisms of crystallization and dissolution of calcium phosphates at surfaces *Glastech Ber Glass Sci* 2000;73(C1):318-325.
- [54] Brohede U, Zhao S, Lindberg F, Mihranyan A, Forsgren J, Stromme M, Engqvist H. A novel graded bioactive high adhesion implant coating. *Applied Surface Science* 2009;255:7723-7728.
- [55] Muller F, Muller L, Caillard D, Conforto E. Preferred growth orientation of biomimetic apatite crystals. *Journal of Crystal Growth* 2007;304:464-471.
- [56] Leng Y, Qu S. TEM examination of single crystal hydroxyapatite diffraction. *J Mater Sci Lett* 2002;21:829-830.
- [57] Lindahl C, Borchardt P, Lausmaa J, Xia W, Engqvist H. Studies of early growth mechanisms of hydroxyapatite on single crystalline rutile: a model system for bioactive surfaces. *J Mater Sci Mater Med* 2010 Aug 1.
- [58] Young RA, Mackie PE. Crystallography of human tooth enamel: initial structure refinement. *Mater Res Bull* 1980;15(1):17-29.
- [59] Li ZY, Lam WM, Yang C, Xu B, Ni GX, Abbah SA, Cheung KMC, Luk KDK, Lu WW. Chemical composition, crystal size and lattice structural changes after incorporation of strontium into biomimetic apatite. *Biomaterials* 2007;28:1452-1460.
- [60] Gross KA, Rodriguez-Lorenzo LM. Sintered hydroxyfluorapatites. Part I: Sintering ability of precipitated solid solution powders. *Biomaterials* 2004;25:1375-1384.
- [61] Robinson C, Shore RC, Brookes SJ, Strafford S, Wood SR, Kirkham J. The Chemistry of Enamel Caries. *Crit Rev Oral Biol Med* 2000;11:481-495.
- [62] Pietak A, Reid J, Stott M, Sayer M. Silicon substitution in the calcium phosphate bioceramics. *Biomaterials* 2007;28: 4023-4032.
- [63] Landi E, Tampieri A, Belmonte MM, Celotti G, Sandri M, Gigante A, Fava P, Biagini G. Biomimetic Mg- and Mg<sub>2</sub>CO<sub>3</sub>-substituted hydroxyapatites: synthesis characterization and in vitro behaviour. *J Euro Ceram Soc* 2006;26:2593-2601.
- [64] Meunier PJ RC, Seeman E, Ortolani S, Badurski JE, Spector TD, Cannata J, Balogh A, Lemmel EM, Pors-Nielsen S, Rizzoli R, Genant HK, Reginster JY The effects of strontium ranelate on the risk of vertebral fracture in women with postmenopausal osteoporosis. *N Engl J Med* 2004;350:459-468.
- [65] Hott M dPC, Modrowski D, Marie PJ. Short-term effects of organic silicon on trabecular bone in mature ovariectomized rats. *Calcified Tissue Int* 1993;53:174-179.
- [66] P.Ammann, V.Shen, B.Robin, MY.auras, J.P.Bonjour, R.Rizzoli. Strontium ranelate improves bone resistance by increasing bone mass and improving architecture in intact female rats. *J Bone Miner Res* 2004;19:2012-2020.

- [67] Wang Y, Zhang S, Zeng X, Ma LL, Weng W, Yan W, Qian M. Osteoblastic cell response on fluoridated hydroxyapatite coatings. *Acta Biomater* 2007;3:191-197.
- [68] M. Y. Role of zinc in bone formation and bone resorption. *J Trace Elem Exp Med* 1998;11:119-135.
- [69] Moonga B, Dempster D. Zinc is a potent inhibitor of osteoclastic bone resorption in vitro. *J Bone Miner Res* 1995;10:453-457.
- [70] Narayanan R, Seshadri SK, Kwon TY, Kim KH. Calcium Phosphate-Based Coatings on Titanium and Its Alloys. *J Biomed Mater Res Part B* 2008;85B:279-299.
- [71] Zhang E, Zou C, Zeng S. Preparation and characterization of silicon-substituted hydroxyapatite coating by a biomimetic process on titanium substrate *Surface & Coatings Technology* 2009;203:1075-1080.
- [72] Xia W, Lindahl C, Persson C, Thomsen P, Lausmaa J, Engqvist H. Changes of surface composition and morphology after incorporation of ions into biomimetic apatite coating. *Journal of Biomaterials and Nanobiotechnology* 2010:Accepted.
- [73] Boyan BD, Hummert TW, Dean DD, Schwartz Z. Role of material surfaces in regulating bone and cartilage cell response. *Biomaterials* 1996 Jan;17(2):137-146.
- [74] Landi E, Tampieri A, Celotti G, Sprio S, Sandri M, Logroscino G. Sr-substituted hydroxyapatites for osteoporotic bone replacement. *Acta Biomaterials* 2007;3:961-969.
- [75] Thian ES, Huang J, Best SM, Barber ZH, Bonfield W. Novel silicon-doped hydroxyapatite (Si-HA) for biomedical coatings: an in vitro study using acellular simulated body fluid. *J Biomed Mater Res B* 2006;76:326-333.
- [76] Yang L, Perez-Amodio S, de-Groot FYFB, Everts V, Blitterswijk CA, Habibovic P. The effects of inorganic additives to calcium phosphate on in vitro behavior of osteoblasts and osteoclasts. *Biomaterials* 2010;31:2976-2989.
- [77] Bracci B, Torricelli P, Panzavolta S, Boanini E, Giardino R, Bigi A. Effect of Mg(2+), Sr(2+), and Mn(2+) on the chemico-physical and in vitro biological properties of calcium phosphate biomimetic coatings. *J Inorg Biochem* 2009;103(12):1666-1674.
- [78] Capuccini C, Torricelli P, Boanini E, Gazzano M, Giardino R, Bigi A. Interaction of Sr-doped hydroxyapatite nanocrystals with osteoclast and osteoblast-like cells. *J Biomed Mater Res* 2009;89A:594-600.
- [79] Zhang E, Zou C. Porous titanium and silicon-substituted hydroxyapatite biomodification prepared by a biomimetic process: characterization and in vivo evaluation. *Acta Biomaterialia* 2009;5(5):1732-1741.



## **Advances in Biomimetics**

Edited by Prof. Marko Cavrak

ISBN 978-953-307-191-6

Hard cover, 522 pages

**Publisher** InTech

**Published online** 26, April, 2011

**Published in print edition** April, 2011

The interaction between cells, tissues and biomaterial surfaces are the highlights of the book "Advances in Biomimetics". In this regard the effect of nanostructures and nanotopographies and their effect on the development of a new generation of biomaterials including advanced multifunctional scaffolds for tissue engineering are discussed. The 2 volumes contain articles that cover a wide spectrum of subject matter such as different aspects of the development of scaffolds and coatings with enhanced performance and bioactivity, including investigations of material surface-cell interactions.

### **How to reference**

In order to correctly reference this scholarly work, feel free to copy and paste the following:

Wei Xia, Carl Lindahl, Jukka Lausmaa and Håkan Engqvist (2011). Biomimetic Hydroxyapatite Deposition on Titanium Oxide Surfaces for Biomedical Application, *Advances in Biomimetics*, Prof. Marko Cavrak (Ed.), ISBN: 978-953-307-191-6, InTech, Available from: <http://www.intechopen.com/books/advances-in-biomimetics/biomimetic-hydroxyapatite-deposition-on-titanium-oxide-surfaces-for-biomedical-application>

# **INTECH**

open science | open minds

### **InTech Europe**

University Campus STeP Ri  
Slavka Krautzeka 83/A  
51000 Rijeka, Croatia  
Phone: +385 (51) 770 447  
Fax: +385 (51) 686 166  
[www.intechopen.com](http://www.intechopen.com)

### **InTech China**

Unit 405, Office Block, Hotel Equatorial Shanghai  
No.65, Yan An Road (West), Shanghai, 200040, China  
中国上海市延安西路65号上海国际贵都大饭店办公楼405单元  
Phone: +86-21-62489820  
Fax: +86-21-62489821

© 2011 The Author(s). Licensee IntechOpen. This chapter is distributed under the terms of the [Creative Commons Attribution-NonCommercial-ShareAlike-3.0 License](#), which permits use, distribution and reproduction for non-commercial purposes, provided the original is properly cited and derivative works building on this content are distributed under the same license.

IntechOpen

IntechOpen